Journal of Water Process Engineering 78 (2025) 108838

Contents lists available at ScienceDirect

Journal of Water Process Engineering

journal homepage: www.elsevier.com/locate/jwpe

Kinetic and mechanistic insights into the photo-Fenton oxidation of polystyrene nanoplastics in water

Jorge Garcia [a,*], Carla di Luca [a,b], Amina Abarkan [a], Laura Cherta [c], Macarena Munoz [a,*], Zahara M. de Pedro [a], Jose A. Casas [a]

[a] Departamento de Ingeniería Química, Universidad Autónoma de Madrid, Ctra. Colmenar km 15 (28049), Madrid, Spain
[b] División Catalizadores y Superficies, Instituto de Investigaciones en Ciencia y Tecnología de Materiales (INTEMA-CONICET), Av. Colón 10850 (7600), Mar del Plata, Argentina
[c] IMDEA Water Institute, University of Alcalá, Av. Punto Com 2 (28805), Madrid, Spain

ARTICLE INFO

Editor: Sadao Araki

Keywords:
Photodegradation
Photo-Fenton
Nanoplastics
Advanced oxidation processes
Water treatment
Polystyrene

ABSTRACT

Microplastics and nanoplastics (NPs) are widespread in aquatic environments and readily accumulate along the food chain. Given their varied sizes in real systems, evaluating degradation processes at various scales is essential for a comprehensive understanding of their fate. In this study, the photo-Fenton degradation of polystyrene (PS) nanospheres with initial particle sizes of D_0 = 140, 252, 460, 909, and 1100 nm was investigated. Oxidation evolution and treatment efficiency were assessed using turbidity and Total Organic Carbon (TOC) measurements, while Transmission Electron Microscopy (TEM) provides insights into particle size and morphological changes. Pyrolysis–Gas Chromatography/Mass Spectrometry (Py-GC/MS) and Ion Chromatography (IC) were used to identify intermediate degradation products. The results demonstrated that smaller particles degraded more rapidly due to their higher surface-to-volume ratio, with complete TOC removal achieved for all particle sizes in relatively short reaction times (40–80 min). The degradation kinetics were accurately described using the Shrinking Core Model and the Prout-Tompkins Model, which revealed distinct stages of reactivity and sigmoid behavior. During the initial activation phase, oxygenated surface groups were incorporated into the PS NPs, followed by chain scission and oxidation into low-molecular-weight aromatic and aliphatic compounds. Finally, these intermediates were fully mineralized into CO_2 and H_2O, leaving no detectable leached by-products or residual NPs.

1. Introduction

Plastics have proven exceptional utility across a wide range of applications owing to their versatile properties, ease of molding into various shapes and sizes, and low production cost. However, this functional diversity has also driven the widespread accumulation of plastic pollution in diverse environmental matrices to become a serious global problem [1]. Once released into the environment, plastic debris undergoes a series of transformation processes, fragmenting into progressively smaller particles such as microplastics (MPs) and nanoplastics (NPs), defined as particles smaller than 5 mm and 1 μm, respectively. Although a size range of 1–100 nm is often used in regulatory contexts for engineered nanomaterials, there is no universal consensus when it comes to nanoplastics. In environmental research, an operational range of 1–1000 nm is commonly adopted to encompass particles that, even above 100 nm, exhibit colloidal properties and environmental behaviors distinct from larger microplastics [2,3]. NPs have been studied less extensively but may pose the greatest risks due to their higher likelihood of crossing biological membranes and disrupting cellular functions [4]. Moreover, NPs have been detected in various ecosystems, and their dispersion is primarily linked to aquatic environments.

Discharges from municipal wastewater treatment plants (WWTPs) are key vectors for introducing MPs and NPs into natural water streams. The number of particles and their morphology or size in the effluent depends on many variables, such as the population served, treatments applied, or the type of wastewater treated [5]. This heterogeneity in wastewater indicates that treatments that are effective for some types of water may not be suitable for others. In addition, it has been found that the treatments used in WWTPs can accelerate the fragmentation of MPs into NPs through photo-oxidative processes, biodegradation, hydrolysis

* Corresponding authors.
E-mail addresses: jorge.garciam@uam.es (J. Garcia), macarena.munnoz@uam.es (M. Munoz).

https://doi.org/10.1016/j.jwpe.2025.108838
Received 17 July 2025; Received in revised form 12 September 2025; Accepted 27 September 2025
Available online 3 October 2025

or mechanical stress rupture [6–8]. Sun et al. [9] evaluated the effectiveness of different WWTPs for the removal of MPs and NPs. The authors stated that plants with only secondary treatment were able to remove approximately 88 % of the plastic particles from the influent, whereas those with tertiary treatment were able to remove up to 97 %. Although these removal levels are high, the large flow rates of treated water indicated that a significant number of particles is continuously discharged into the receiving medium. Therefore, the continuous generation of NPs, their incomplete removal and subsequent emission from the WWTP current treatments represents a challenge on a global scale [10,11]. In this context, the scientific community is increasingly focusing on the development of innovative treatment technologies that allow the complete removal of these solid pollutants.

Advanced oxidation processes (AOPs) are promising candidates for the elimination of persistent and non-biodegradable organic pollutants from water. These processes, based on the in-situ generation of strong reactive oxygen species (ROS), enable the decomposition of pollutants into low-molecular-weight intermediates, ultimately leading to complete oxidation into CO_2 and H_2O [12]. Recently, AOPs have been proposed for the abatement of MPs and NPs in aqueous streams, although the research field is recent [13]. Many publications have reported relatively subtle changes that include superficial modifications, such as cracks, wrinkles, and protuberances, but even the collateral generation of NPs, and the modification of the sorption capacity [8,14–16]. On the other hand, some technologies have proven to be quite effective, however, few studies evaluate the degree of mineralization achieved or investigate the possible formation of smaller MPs and NPs, which represents a critical gap from an environmental point of view, given the potential toxicity and greater mobility of oxidation intermediates, their interactions with natural matrices (including soil organic matter), triggering the need to assess possible effects on ecosystems [17]. Building on this, Li et al. [18] applied ozonation for the removal of PS NPs (100 nm), reported a mineralization yield of 43 % in 4 h. In the same line, Hidayaturrahman et al. [19] demonstrated that the implementation of ozonation as tertiary treatment in WWTPs resulted in the reduction up to 99 % of MPs present in wastewater. It has also been shown that photocatalytic processes are effective, with 72 % elimination of HDPE (~700 μm), in 50 h using a carbon- and nitrogen-doped TiO_2 catalyst [20]. Metal and non-metal doping (Ag-TiO_2/TiO_2) has also shown excellent results in the removal of PS MPs (100–250 μm), reaching 100 % mass loss in 2 h reaction time [21]. Similarly, the electro-peroxidation process has demonstrated remarkable efficiency, achieving complete removal of PS NPs in just 40 min in laundry wastewater spiked with NPs [22]. Fenton and Fenton-like technologies have also received considerable attention. In a recent study, Ortiz et al. [23] applied the homogeneous Fenton process to the removal of MPs and NPs of different nature, achieving mass losses of up to 20 % for MPs, whereas NPs accomplished mineralization levels of up to 70 % in 7.5 h reaction time at 80 °C. Following up on this research, the intensification of the conventional Fenton process (i.e., *dark Fenton*) using a UV–Vis lamp demonstrated the efficiency of the photo-Fenton process for the complete mineralization of PS NPs in only 40 min reaction time operating at ambient conditions [24,25]. The oxidation process in the photo-Fenton system is driven mostly by the generation of hydroxyl radicals (HO·) [26]. Initially, ferric ions (Fe^{3+}) are photoreduced to ferrous ions (Fe^{2+}) under UV–Vis irradiation (Eq. (1)), which initiates the catalytic cycle [27]. Fe^{2+} reacts with H_2O_2 to produce HO· via the Fenton reaction (Eq. (2)), while Fe^{3+} can also react with H_2O_2 to form hydroperoxides (HOO·), regenerating ferrous species (Eq. (3)). In addition, if the lamp provides enough irradiation energy (i.e., appropriate wavelength and intensity), H_2O_2 can decompose directly under photolysis, generating HO· (Eq. (4)). However, the direct formation of HO· from the photolysis of water requires UV irradiation in a vacuum (<190–195 nm) and is not expected under our experimental conditions (lamp emission 200–600 nm) [28,29]. These reactions sustain a continuous catalytic cycle, ensuring a constant generation of radicals and enhancing the oxidation of pollutant [30–32].

$$Fe^{3+} + H_2O + h\nu \rightarrow Fe^{2+} + H^+ + HO\cdot \quad (1)$$

$$Fe^{2+} + H_2O_2 \rightarrow Fe^{3+} + HO\cdot + OH^- \quad (2)$$

$$Fe^{3+} + H_2O_2 \rightarrow Fe^{2+} + HOO\cdot + H^+ \quad (3)$$

$$H_2O_2 + h\nu \rightarrow 2HO\cdot \quad (4)$$

As mentioned above, a previous study by our group has already demonstrated the complete mineralization of polystyrene nanoplastics (140 nm) under ambient conditions [24]. In a complementary work, methodological strategies were evaluated and discussed to monitor the advanced oxidation of nanoplastics in water [25]. More recently, the kinetic behavior of the system was successfully described by simple mathematical expressions based on the Shrinking Core Model and the Prout-Tomkins Model [33]. Together, these contributions established both the technical feasibility and methodological framework required to advance research on the photo-Fenton degradation of nanoplastics in water. In line with our previous works, this study takes a significant step forward in understanding the removal of NPs of different sizes, with a focus on assessing the efficiency of the photo-Fenton process. The novelty of this work lies in the systematic evaluation of particle size effects and their influence on degradation efficiency, kinetic behavior, and reaction mechanisms. For this purpose, the effect of particle size was thoroughly examined using various PS NPs samples, ranging from 140 to 1100 nm (140, 252, 460, 909, and 1100 nm), as model pollutants. The evolution of the oxidation level was followed through turbidity measurements of the reaction medium and complemented by particle size analysis using TEM imaging. The degradation kinetics were subsequently analyzed using the Shrinking Core Model (SCM) and the Prout-Tompkins Model (PTM) to provide simple mathematical expressions to describe the degradation behavior of PS NPs. To deepen the understanding of the reaction mechanisms, the intermediates generated during the photo-oxidation process were identified using Pyrolysis-Gas Chromatography/Mass Spectrometry (Py-GC/MS) and Ion Chromatography (IC), gaining insight on the oxidation pathways involved. Finally, the mineralization of PS NPs and their leached intermediates was also evaluated through Total Organic Carbon (TOC) measurements. Overall, the results showed that the photo-Fenton process achieved complete mineralization of PS nanoparticles in short reaction times (40–80 min). Smaller particles degraded more rapidly due to their higher surface-to-volume ratio, and the process was satisfactorily described by the SCM and PTM kinetic models. Oxidation intermediates (polycyclic aromatic compounds and short-chain acids) were detected by Py-GC/MS and IC, but these compounds were completely mineralized into CO_2 and H_2O, leaving no persistent by-products or residual NPs in the treated water.

2. Materials and methods

2.1. Materials and chemicals

Five commercial monodisperse PS NPs samples, PS-R-KM248 (140 ± 5 nm, 5 % *w/v*), PS-R-KM239 (252 ± 5 nm, 5 % w/v), PS-R-KM378 (460 ± 10 nm, 5 % w/v), PS-R-KM123 (909 ± 27 nm, 5 % w/v), and PS-R-KM265 (1100 nm ± 30 nm, 10 % w/v), were purchased from MicroParticles GmbH. Throughout this study, the samples were denoted as PS140, PS252, PS460, PS909, and PS1100, respectively and their main characteristics are summarized in Table 1, which also presents the theoretical oxidation stoichiometry, including the reaction equation and the required H_2O_2 dose for complete mineralization.

Nitric acid (65 %), titanium (IV) oxysulfate (>99 %), and iron (III) nitrate nonahydrate (98 %) were obtained from Sigma-Aldrich. Hydrogen peroxide solution (33 % *w/v*) was supplied by Panreac. All compounds were used as received without further purification. Deionized water was used in all the experiments (Milli-Q system, 18.2 MΩ·cm, TOC < 50 ppb).

Table 1
Main characteristics of PS NPs tested in this work and the theoretical stoichiometry for their complete oxidation.

	PS NPs
Molecular structure	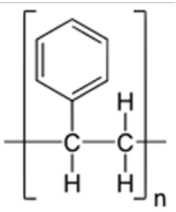
TEM images	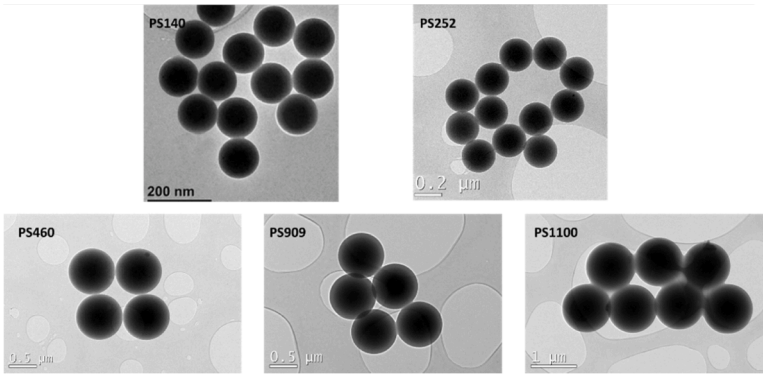
Melting point (°C)	74–105
Oxidation reaction	$[C_8H_8]_n + 20{\cdot}n\ H_2O_2 \rightarrow 8{\cdot}n\ CO_2 + 24{\cdot}n\ H_2O$
H_2O_2 (mg L^{-1})[a]	130

[a] Theoretical stoichiometric dose of H_2O_2 for the complete oxidation of $[PS\ NPs]_0 = 20$ mg L^{-1}.

2.2. Oxidation experiments

The experimental setup consisted of an immersion-wall batch-jacketed photoreactor (0.7 L working volume, 0.8 L total capacity) made of borosilicate glass. A 150 W medium-pressure mercury lamp (Peschl Ultraviolet, UV–Vis Nova Light TQ-150) was positioned inside a centrally immersed quartz sleeve at an intermediate height relative to the liquid column, ensuring uniform irradiation of the suspension. The lamp emitted between 200 and 600 nm (Fig. S1), with an irradiance of 200 W m^{-2} in the UV-C region, as measured using a photo-radiometer (Delta Ohm, model HD 2102.1). Temperature was controlled by a heating plate, which also provided continuous magnetic stirring (IKA RCT Basic, Germany). For safety reasons, the photoreactor was placed inside a protective box, and all reagents were dosed from outside. Photo-Fenton experiments were carried out under previously optimized conditions [24,25]: $[PS\ NPs]_0 = 20$ mg L^{-1}, $[Fe^{3+}] = 1$ mg L^{-1}, $[H_2O_2]_0 = 130$ mg L^{-1}, with additional doses of 130 mg L^{-1} supplied every 20 min to compensate for H_2O_2 depletion during the reaction, $T = 25$ °C, $pH_0 = 3$, and a stirring rate of 500 rpm. The pH remained nearly constant throughout the reaction (final pH ≈ 2.8), thereby ensuring optimal conditions for the photo-Fenton process. All experiments were carried out in triplicate and the corresponding standard deviations are shown as error bars in the figures. A detailed description of the experimental sequence and reagent dosing strategy is provided in the Supplementary Material.

2.3. Analytical methods

It is important to highlight that all the NPs tested formed stable colloidal suspensions in water. Accordingly, the progression of the oxidation reactions was monitored by analyzing the turbidity of the samples using a turbidimeter (Hanna Instruments, HI88713). The final stages of the oxidation reactions were also assessed by Total Organic Carbon (TOC) measurements using a Shimadzu TOC-L analyzer to evaluate the mineralization yield achieved. Further details on calibration procedures for turbidity and TOC analyses are provided in the Supplementary Material. H_2O_2 and dissolved iron concentrations were quantified by standard colorimetric methods using a UV–Vis spectrophotometer (Shimadzu, UV 2100) [34,35]. Transmission electron microscopy (TEM) using a JEOL JEM 2100 with 0.17 nm resolution was employed by the authors to determine the evolution of particle size during the oxidation assays. The micrographs were processed using the ImageJ software, allowing for particle counting and diameter measurements at each selected reaction time (more than 100 particles per sample were considered when possible). For the detection of photo-Fenton oxidation by-products, a pyrolyzer 6200 (CDS Analytical) coupled with a gas chromatography–mass spectrometry system (7890 B and 5977 B MSD, Agilent Technologies) was utilized (Pyr-GC–MS). An HP-5 capillary column (Agilent Technologies) was used, with helium as the carrier gas. A synthetic polystyrene standard was analyzed under identical conditions to confirm the identity of pyrolytic fragments. By-products were identified by comparing the obtained spectra with a NIST Mass Spectral Library, without the use of additional synthetic standards. Additionally, the final products were analyzed by ion chromatography (Metrohm 790 IC) with conductivity detector, using a 3.2 mM Na_2CO_3 solution as mobile phase and a Metrosep A Sup 5–250 column (25 cm length, 4 mm internal diameter, 5 µm particle size) as stationary phase.

3. Results and discussion

3.1. Impact of nanoplastics size

The individual contributions of light, Fe^{3+}, and H_2O_2 within the photo-Fenton system were thoroughly assessed in a previous study by our group [24]. That work demonstrated that control experiments tested UV, UV/Fe^{3+}, UV/H_2O_2 and Fenton (H_2O_2/Fe^{3+}), led to negligible degradation of PS NPs, confirming that only the photo-Fenton cycle

ensures effective removal. Instead, the present work focuses on evaluating the effect of particle size on the overall photo-Fenton degradation of PS nanoparticles. Five PS NPs samples with different nominal diameters ranging from 140 to 1100 nm were used to evaluate the effect of particle size on their photo-Fenton degradation. Fig. 1A shows the evolution of turbidity as a general indicator of PS NPs degradation upon the photo-Fenton treatment. As observed, an increase in particle size required a longer reaction time to achieve the complete removal of PS NPs. For instance, while PS140 particles were completely degraded within 40 min reaction time, PS1100 required almost 80 min.

The influence of the particle size can be related to the surface-to-volume (S/V) ratio of the particles (Fig. 1B and Table S1). Larger particles have a lower S/V ratio, which results in less surface area available for interaction with reactive oxygen species (ROS) generated during the process. In contrast, smaller particles, with a higher S/V ratio, provide a larger surface area for interaction with ROS, leading to faster degradation [36]. In fact, largest particles exhibited a short initial induction period, during which turbidity reduction was minimal. This may be due to the gradual incorporation of oxygen-containing groups on the particles surface, which is necessary for the progression of NPs degradation. As described in the literature, this observation suggests that NPs oxidation begins at the surface, where UV-C light and oxygenated radicals interact with the polymer, activating the particle surface before progressing towards the core [33,37].

To evaluate the evolution of both particle size and morphology, TEM images were acquired throughout the oxidation tests. As a representative example, Fig. 2 shows the results obtained in the oxidation of PS252 (see Fig. S2 to S5 for the other NPs evaluated). Table S2 summarizes the evolution of the mean particle diameter and the percentage of volume reduction. In general, as the reaction advances, a progressive reduction in particle size was observed, further confirming that oxidation occurs from the surface to the core of the particles. The oxidation process was also accompanied by the formation of particle aggregates [38] as can be seen in Fig. 2A.

Initially ($t = 0$ min), PS NPs displayed a spherical morphology and homogeneous particle size (Fig. 2). However, as photo-oxidation progresses, significant diminution of this size was observed, reflecting the interactions between ROS and the polymer surface. For instance, after 20 min of reaction time, PS140 (Fig. S2) decreased in size to about 99.5 nm, corresponding to a volume reduction of 62 %. In contrast, larger particles like PS1100 showed a smaller particle size reduction (Fig. S5), shrinking to 1035 nm, which only represented an 18 % reduction in volume. This indicates that the degradation of larger nanoparticles is slower and less obvious at first. By 30 min, the degradation process accelerated significantly, with smaller particles shrinking rapidly and nearing complete elimination (Figs. 1, 2, S2, S3). For instance, more than 90 % volume reduction was achieved with PS252. Again, larger particles continued to degrade at a slower but steady rate (Figs. S4, S5). In all cases, particle size reduction was relatively slow at the beginning and then accelerated. This reaction regime is likely due to the incorporation of oxygenated groups at the PS NPs surface, activating the solid particles and facilitating the polymeric chain breakdown [24]. Notably, despite the surface attack by ROS, the particles maintained their spherical morphology unchanged throughout reaction regardless of their size. This fact seems to be due to the high homogeneity of the polymer matrix and the uniform oxidative attack across the surface preventing any significant deformation. As a result, the shape remains consistent while the particle size gradually reduces (Figs. 2B, S2-S5).

To gain further insights into the degradation yield of PS NPs, the TOC of the final effluents was analyzed after achieving total turbidity removal. The initial TOC concentration was 19.6 mg L^{-1}, corresponding to the organic load of the PS suspensions. In all cases, complete mineralization was found (40–80 min, depending on particle size), confirming that no refractory by-products, either solid or dissolved, were formed during the oxidation process. These results highlight the potential of the photo-Fenton process not only for polymer degradation but for complete oxidation into carbon dioxide and water. Comparable studies using other AOPs have reported only partial mineralization: Cai et al. [39] achieved ≈94 % turbidity reduction for PS NPs (50–100 nm, 5 mg L^{-1}) after 360 min with UV/PMS, but only ~64 % TOC decrease. Similarly, Ye et al. [40] obtained ≈95 % removal for PS NPs (≈120 nm, 20 mg L^{-1}) by electro-Fenton after 6 h, with ≈74 % TOC reduction. This aspect is crucial since the mere decrease of NPs particle size could be even more harmful for the environment, as smaller particles are more readily absorbed by biological membranes, potentially impairing cellular functions [41].

3.2. Kinetic analysis of nanoplastics degradation in water

The evolution of nanoparticles (NPs) is a complicated process involving several specific steps. First, there is an initial phase of oxidation and surface activation that takes place relatively slowly. This stage modifies the properties of the nanoparticle and sets the stage for the next phase: the progressive reduction of its diameter, which accelerates as the particle becomes smaller. Because this process involves multiple mechanisms and reaction rates that vary throughout its evolution, it cannot be adequately described by a simple first-order equation. This model is too limited to capture the complex sequence of chemical and physical transformations that occur during surface oxidation and size reduction. For this reason, it is essential to use more complete and

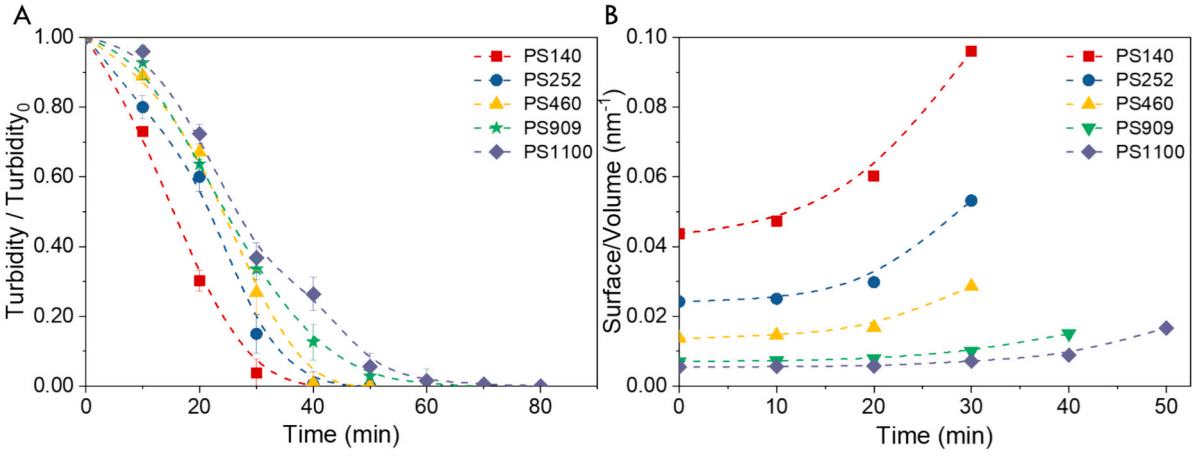

Fig. 1. Effect of particle size upon photo-Fenton oxidation of PS NPs: A) Turbidity; and B) Surface-to-volume ratio (S/V) of PS NPs determined from TEM images. The S/V ratio was calculated from the average particle diameters, assuming spherical geometry. The dashed lines represent the trend of curves. Operating conditions: [PS NPs]$_0$ = 20 mg L^{-1}; [Fe^{3+}]$_0$ = 1 mg L^{-1}; [H_2O_2]$_0$ = 130 mg L^{-1} (multiple dosages of 130 mg L^{-1}, every 20 min); pH $_0$ = 3; and T = 25 °C.

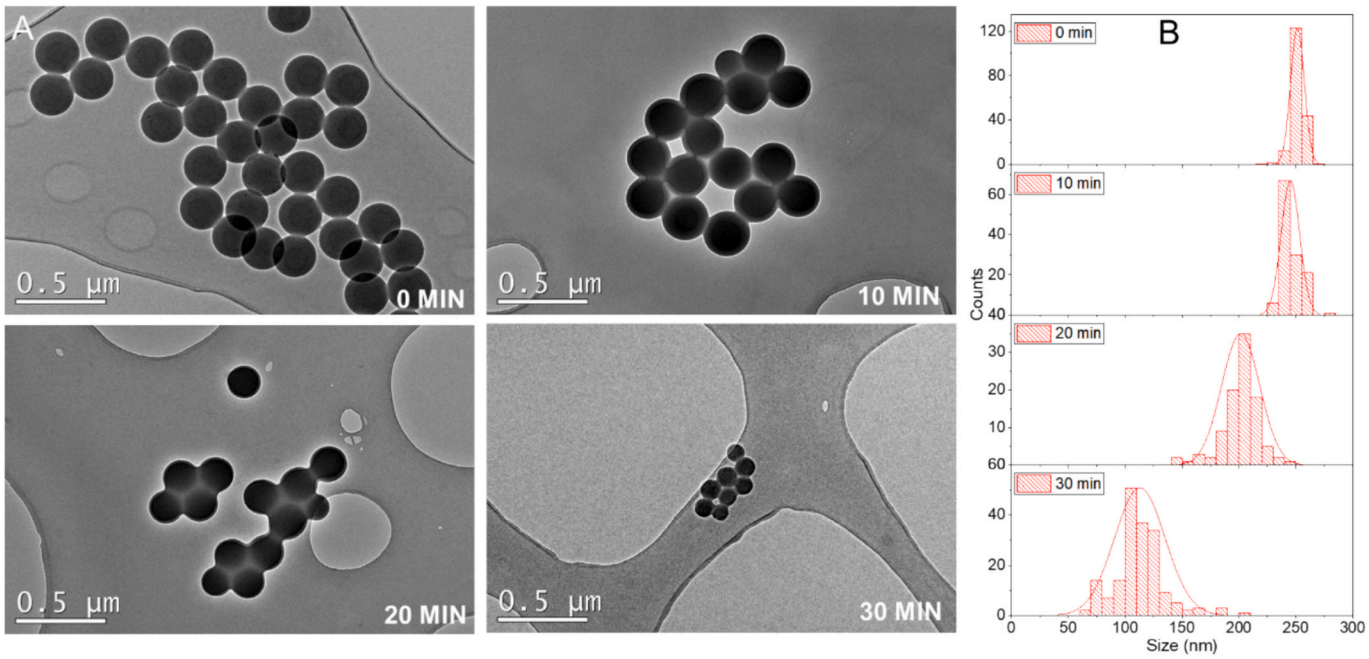

Fig. 2. Evolution of particle size upon photo-Fenton treatment of PS NPs: A) TEM images; and B) Particle size distribution. Operating conditions: $D_0 = 252$ nm, $[PS\ NPs]_0 = 20$ mg L^{-1}; $[Fe^{3+}]_0 = 1$ mg L^{-1}; $[H_2O_2]_0 = 130$ mg L^{-1}, dosed every 20 min; pH $_0 = 3$; and $T = 25$ °C.

sophisticated kinetic models that can represent the different stages into which the process is divided and more accurately reflect the real dynamics of nanoparticle evolution, such as Shrinking Core Model and Prout Tompkins Model.

3.2.1. *Shrinking core model*

Solid-fluid reaction models such as the Shrinking Core Model (SCM) represent an ideal approach to fit the evolution of PS NPs oxidation. In a previous work, di Luca et al. [33] demonstrated that SCM allows to fit accurately the photo-Fenton oxidation of PS NPs under different operating conditions. It was found that the degradation of NPs is governed by chemical reaction control, with no external diffusion limitations, as also demonstrated by the excellent agreement of the experimental data with a reaction-controlled shrinking core model ($R^2 > 0.99$). In this study, we will delve deeper into the impact of particle size on its oxidation process. The photo-oxidative process is divided into two distinct phases: an initial slower phase, during which surface functionalities are formed and the surface becomes activated, followed by a rapid propagation phase characterized by an accelerated degradation rate and a significant reduction in particle size until complete disappearance. Eq. (5) describe the conversion of solid pollutants (X_B) as a function of the time required for complete conversion (τ),

$$1 - (1 - X_B)^{1/3} = \frac{t}{\tau} \tag{5}$$

Fig. 3 (see Figs. S6 to S9 of the Supplementary Material for other PS NPs sizes) and Table S3 present the kinetic parameters obtained from fitting the SCM to the experimental data together with the corresponding ANOVA results. Assuming the absence of diffusional limitations and that the process proceeds under chemical reaction control, the R^2 values were above 0.96 regardless of the PS NPs size, confirming the applicability of the SCM to this system (Fig. 4). In addition, ANOVA analysis

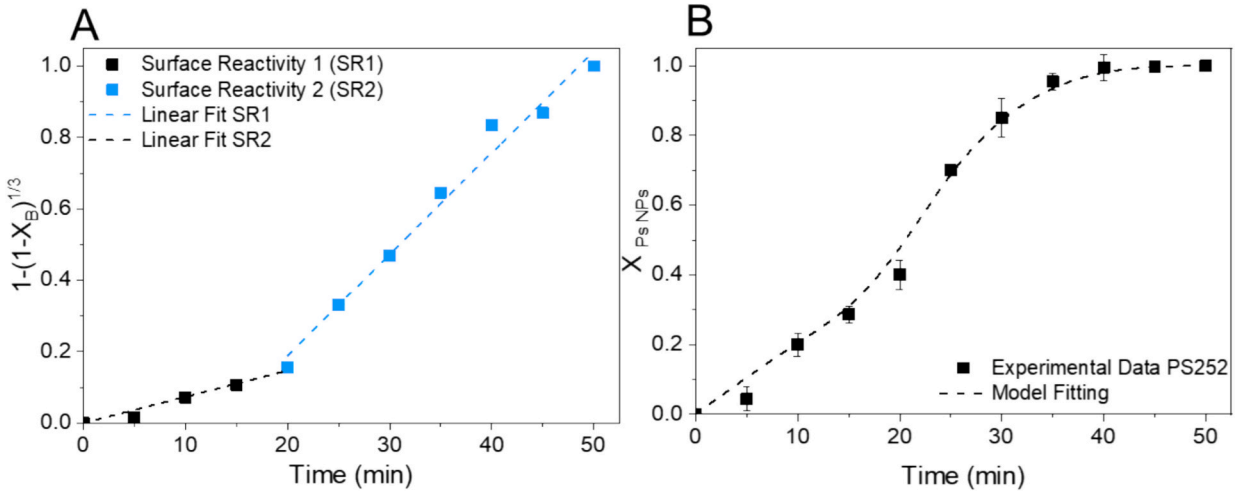

Fig. 3. Evaluation of the Shrinking-Core Model for the photo-Fenton degradation of PS NPs: A) Verification of the model applicability considering two surface reactivities (SR1 and SR2), and B) conversion of PS NPs and model fitting. Operating conditions: $D_0 = 252$ nm, $[PS\ NPs]_0 = 20$ mg L^{-1}; $[Fe^{3+}]_0 = 1$ mg L^{-1}; $[H_2O_2]_0 = 130$ mg L^{-1}, dosed every 20 min; pH $_0 = 3$; and $T = 25$ °C.

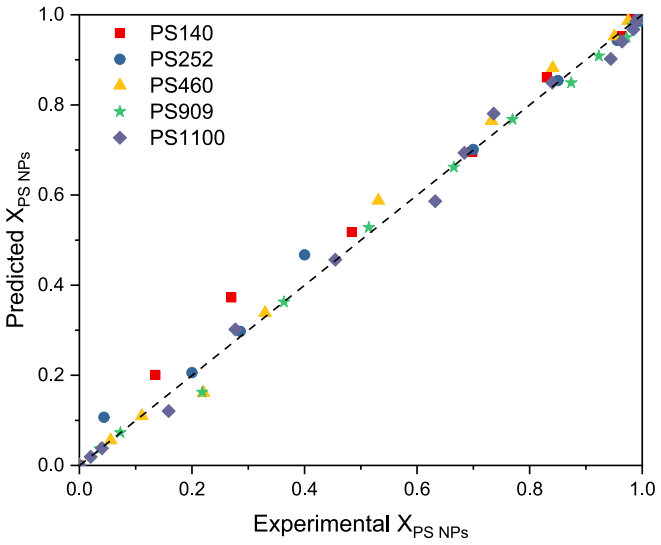

Fig. 4. SCM parity plot comparing model-predicted values and experimental data for the conversion of PS nanoparticles across the studied size range under photo-Fenton oxidation conditions.

showed that all regressions were statistically significant ($p < 0.01$), with F values ranging from ≈ 100 for PS140 up to $>10^5$ for PS1100, which further validates the robustness of the fittings. The kinetic parameters clearly reflect the variation in photo-oxidation rates between the first and second stages of the process. As shown in Table S3, the kinetic rate constants (k_1 and k_2) and the times for complete conversion (τ_1 and τ_2) for each stage are strongly influenced by particle size. Larger particles exhibit slower reaction rates, as indicated by decreasing k_1 and k_2 values, and require longer reaction times (τ_1 and τ_2) for complete conversion. For instance, PS140, with smaller particle size than PS909, allows more efficient interaction with radicals, resulting in higher kinetic rate constant ($k_1 = 0.0144$ min^{-1} and $k_2 = 0.031$ min^{-1}), as well as shorter conversion times ($\tau_1 = 69.44$ min, $\tau_2 = 32.36$ min). Conversely, PS909, with larger particle size, shows lower rate constant values ($k_1 = 0.0025$ min^{-1}, $k_2 = 0.0165$ min^{-1}) and longer conversion times ($\tau_1 = 400$ min, $\tau_2 = 59.52$ min). Again, all these results can be explained by the S/V ratio: smaller particles, with a higher proportion of reactive surface relative to their volume, facilitate greater interaction with radicals, thereby accelerating photo-oxidation. Conversely, larger particles have a lower reactive surface area, limiting the reaction rate. Beyond numerical accuracy, SCM provides a mechanical view of the degradation process: by explicitly assuming control of the chemical reaction, it links the observed kinetics with the progressive reduction of solid particles and allows the two stages of nanoplastics oxidation to be rationalized in terms of surface reactivity and particle size.

3.2.2. *Prout-Tompkins model (PTM)*

The PTM is widely used to describe autocatalytic kinetic reactions. It is particularly relevant for systems that exhibit an initial induction period, resulting in sigmoidal conversion-time curves (i.e., S-shape) [33,42,43]. This behavior is characteristic of NPs degradation, as previously described. Accordingly, this model was applied to fit the experimental data, using Eq. (6), which presents the conversion-time equation proposed in the PTM where k is the kinetic rate constant (min^{-1}), and c denotes the intercept.

$$ln\left(\frac{X_B}{1-X_B}\right) = kt - c \quad (6)$$

The values of the rate constants are collected in Table S4, which also includes the ANOVA statistics. As a representative example, the fitting of the model to the experimental data obtained in the oxidation of PS252 can be seen in Fig. 5 (see Figs. S10 to S13 of the Supplementary Material for other PS NPs sizes). Clearly, the model successfully described the experimental data, with R^2 values above 0.96 regardless of the NPs size (complete set of regression metrics for all fittings is provided in the Supplementary Material, Table S4). To further validate these fittings, ANOVA analysis confirmed that all regressions were statistically significant ($p < 10^{-5}$), with F values ranging from ≈ 200 to nearly 2000 depending on particle size. These consistently high R^2 values, supported by the ANOVA results, demonstrate that PTM reliably captures the main degradation kinetics. This strong agreement confirms the suitability of the model for describing the sigmoidal degradation behavior of PS NPs and provides confidence in the mechanistic interpretation across the entire particle size range studied. This agreement is also illustrated in the parity plot shown in Fig. 6, which compares the values predicted by the model with the experimental data across the range of NP sizes evaluated. Consistent with previous observations, the results obtained with PTM indicate a progressive decrease in the kinetic rate constants as NP size increases from 140 to 1100 nm.

Both the SCM and PTM models have been shown to successfully describe the degradation kinetics of PS nanoparticles through photo-Fenton oxidation. The SCM considers two stages with their respective

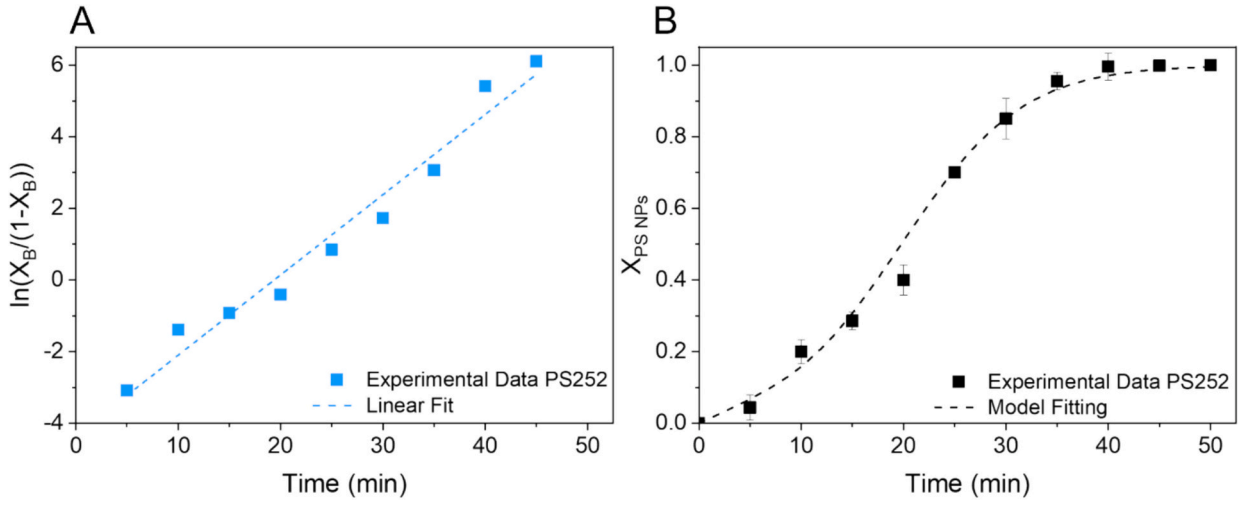

Fig. 5. Assessment of the Prout-Tompkins model for the photo-Fenton degradation of PS NPs: A) Verification of model applicability, and B) Conversion of PS NPs and model fitting. Operating conditions: $D_0 = 252$ nm, $[PS\ NPs]_0 = 20$ mg L^{-1}; $[Fe^{3+}]_0 = 1$ mg L^{-1}; $[H_2O_2]_0 = 130$ mg L^{-1} (multiple dosages of 130 mg L^{-1}, every 20 min); pH $_0 = 3$, and $T = 25$ °C.

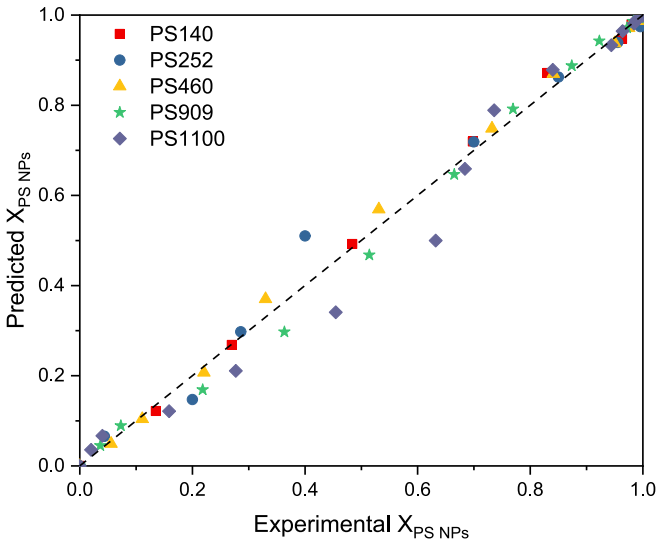

Fig. 6. PTM parity plot comparing model-predicted and experimental data for the conversion of PS nanoparticles across the studied size range under photo-Fenton oxidation conditions.

kinetic rate constants, providing a detailed description of each degradation phase. In contrast, the PTM, with its sigmoidal (S-shaped) curve, integrates the entire process into a single overall rate constant. Apart from the correlation coefficients, the ANOVA results confirmed the statistical significance of all fits ($p < 0.01$ for SCM and $p < 10^{-5}$ for PTM), with consistently high F values across different NPs sizes. While the SCM offers a mechanical view by separating the initiation and propagation stages, the PTM provides an overall correlation, supporting its suitability as a global kinetic descriptor. Taken together, these results indicate that both models are valid and complementary: the PTM is more suitable for describing global kinetics, while the SCM is valuable for the mechanical interpretation of two-stage behavior.

3.3. Photo-oxidation mechanism of polystyrene nanoplastics

To elucidate the reaction mechanism underlying the photo-Fenton oxidation of PS NPs, the experimental conditions were slightly modified to facilitate the identification of the main intermediates generated during the degradation process. Specifically, the initial concentration of PS NPs was significantly increased ($[PS\ NPs]_0 = 100$ mg L^{-1}; $[Fe^{3+}]_0 =$ 1 mg L^{-1}; $[H_2O_2]_0 = 1000$ mg L^{-1} (administered in multiple doses of 500 mg L^{-1}, added every 20 min); pH $_0 = 3$ and $T = 25$ °C). As the primary goal was to identify the dissolved intermediates released into the aqueous phase, the smallest PS NPs ($D_0 = 140$ nm) were selected for this study. Samples were periodically collected and preconcentrated (10-fold) before being analyzed by Py-GC/MS to follow the generation of reaction intermediates.

In addition to the intermediates identified in this work, a comprehensive review of the available literature was conducted to provide a broader overview of the main reactions involved in the photo-Fenton oxidation of PS NPs [37,44–46]. This process is characterized by a complex mechanism that combines UV light-induced photo-oxidation and the attack of hydroxyl radicals (HO·) generated in the photo-Fenton cycle (Eqs. (1), (2) & (4)). In practice, it follows a typical radical

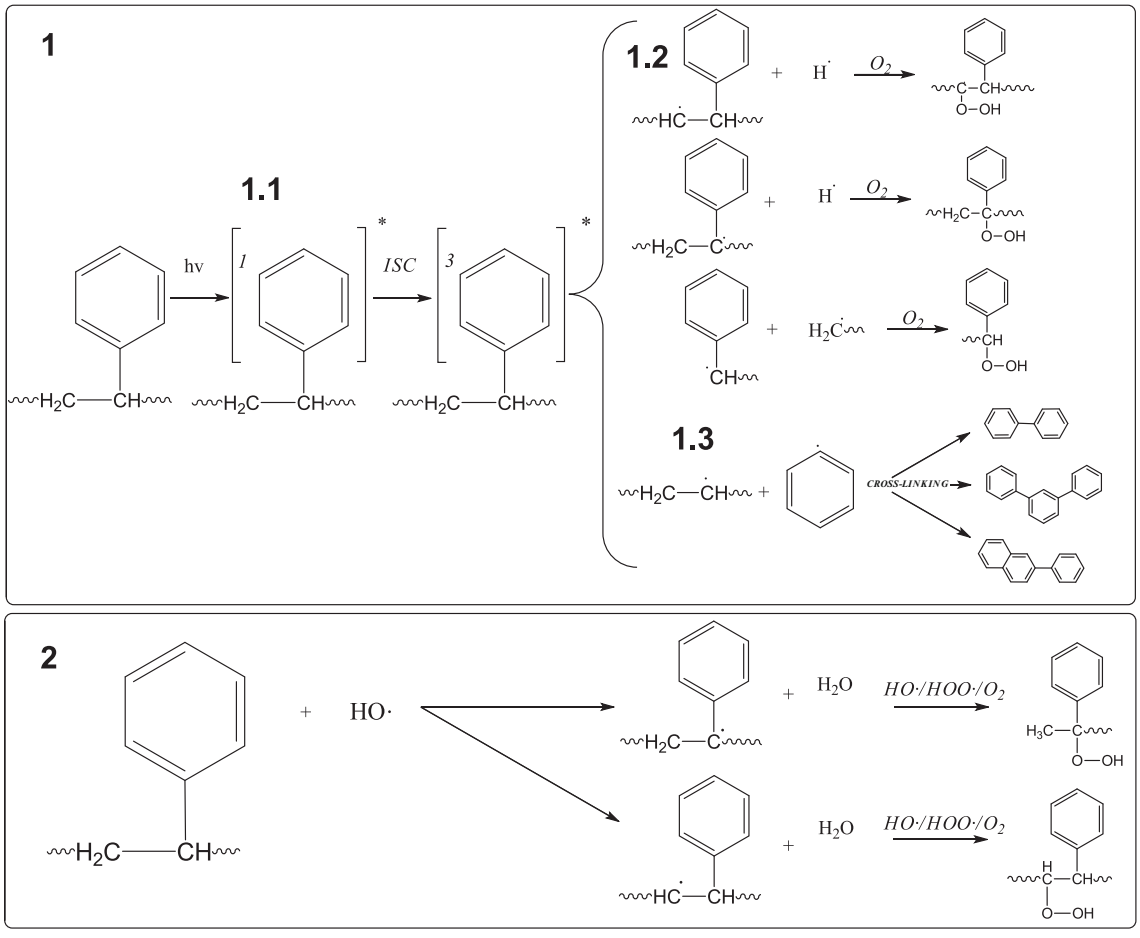

Fig. 7. Initiation pathways of polystyrene degradation upon photo-Fenton treatment: (1) Photolysis and (2) HO· attack.

mechanism, consisting of three key steps: initiation, propagation, and termination. In all these stages, photolysis and ROS drive the formation of both intermediate and final reaction products [37].

The initiation stage includes two main routes: the photolysis of PS (Fig. 7 (1)) and the initial attack of hydroxyl radicals (Fig. 7 (2)). In the photolysis pathway, the irradiation of PS with UV light in the absorption band of the phenyl group ($\lambda \approx 260$ nm) excites the molecule generating a singlet electronic state (S1) which is rapidly converted into a triplet state (T1) through an intersystem crossover (ISC) mechanism, as reported in the literature (Fig. 7 (1.1)) [33,37]. The instability of the excited state leads to intramolecular energy transfer to the C—H or C—C bonds in the polymer chain, resulting in the formation of alkyl radicals at secondary or tertiary carbon positions (Fig. 7 (1.2)). Additionally, cleavage of the C—C bond connecting the aromatic ring to the aliphatic chain can occur, generating further radical species. In successive steps, these radicals may recombine, ultimately leading to the formation of cross-linked structures (Fig. 7 (1.3)). This hypothesis was supported by Py-GC/MS analysis, which detected polycyclic aromatic hydrocarbons such as *m*-terphenyl, biphenyl, and 2-phenylnaphthalene (Figs. S14 to S16), produced by the recombination of radicals through resonance mechanisms [46,47]. Simultaneously, UV irradiation activates the photo-Fenton cycle where hydrogen peroxide (H_2O_2) is decomposed leading to the generation of hydroxyl radicals (Eq. (4)). These oxidizing species directly attack the PS chains generating carbon-centered radicals in secondary and tertiary positions of the chain (Fig. 7 (2)) [36,48–50]. In both pathways (1 and 2), radicals react with oxygenated species present in water to form peroxides, initiating the propagation stage.

In the propagation stage, the generated radicals participate in chain reactions leading to the formation of surface oxygen groups and fragmentation of polymeric chains. The alkyl radicals react with molecular oxygen to form peroxide radicals. Subsequently, the peroxide radicals extract hydrogens from neighboring PS chains forming hydroperoxide groups (Fig. 8 (3)) [46]. Under UV irradiation, hydroperoxides groups decompose (via homolytic cleavage of the O—O bond) into alkoxy groups and hydroxyl radicals [46,51]. At this point, the fate of the alkoxy radicals follows two types of beta-scission reactions. The first pathway leads to the formation of phenol when the cleavage occurs at the carbon attached to the aromatic ring (Fig. 8 (3.1)). However, part of this pathway may lead to crosslinking reactions before phenol formation, which could explain the absence of this compound among the analyzed by-products. Additionally, the released phenol molecule might be rapidly oxidized under similar operating conditions tested in this study [52]. Consequently, this pathway appears to be of marginal significance under our experimental conditions. Conversely, when cleavage occurs in the aliphatic chain at a secondary or tertiary carbon, the resulting radicals lead to the formation of carbonyl and ketone compounds (Fig. 8 (3.2)), specifically phenylacetaldehyde (from a tertiary carbon; Fig. 8 (3.2.1)) and acetophenone (from a secondary carbon; Figs. 8 (3.2.2) & S17). Furthermore, it is possible that some of these ketone groups recombine with other by-products, resulting in the formation of compounds with multiple aromatic rings, such as the chalcone identified (Fig. S18) among the by-products in our analysis and literature [46,53]. Additionally, benzaldehyde and benzoic acid were also detected in our analysis (Figs. S19 & S20), further supporting this degradation pathway and indicating the end of the propagation stage.

Finally, in the termination stage, carbonyl groups and ketones undergo further reactions with UV light and hydroxyl radicals (Fig. 9(4)). While pathways involving the decarboxylation of the carboxylic and ketonic groups in benzoic acid and acetophenone are possible [54,55], they appear improbable due to the absence of phenolic compounds, such as phenol and quinones, among the detected products. This observation suggests that the predominant mechanism of HO· attack involves successive hydroxylations of both compounds, leading to the formation of hydroxylated intermediates. These intermediates ultimately undergo ring opening and cleavage, resulting in the formation of oxygenated aliphatic compounds such as malonic, oxalic, formic, and acetic acid

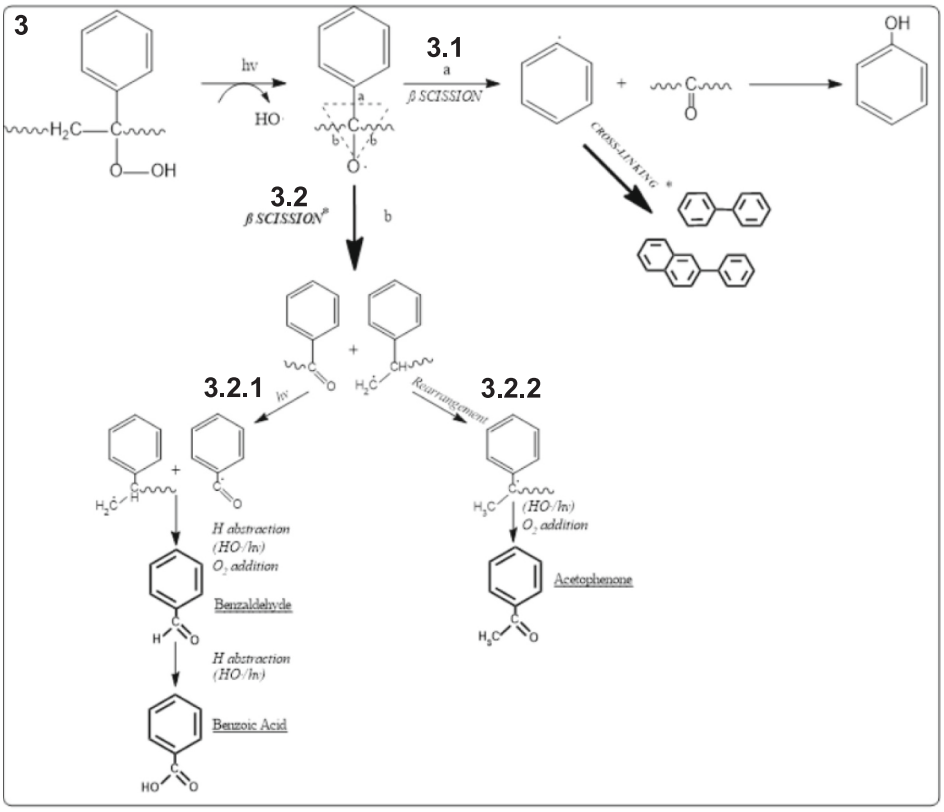

Fig. 8. Propagation mechanism of polystyrene degradation upon photo-Fenton treatment. The molecules in bold represent the detected compounds in this work. The bold arrow indicates the preferred reaction pathway.

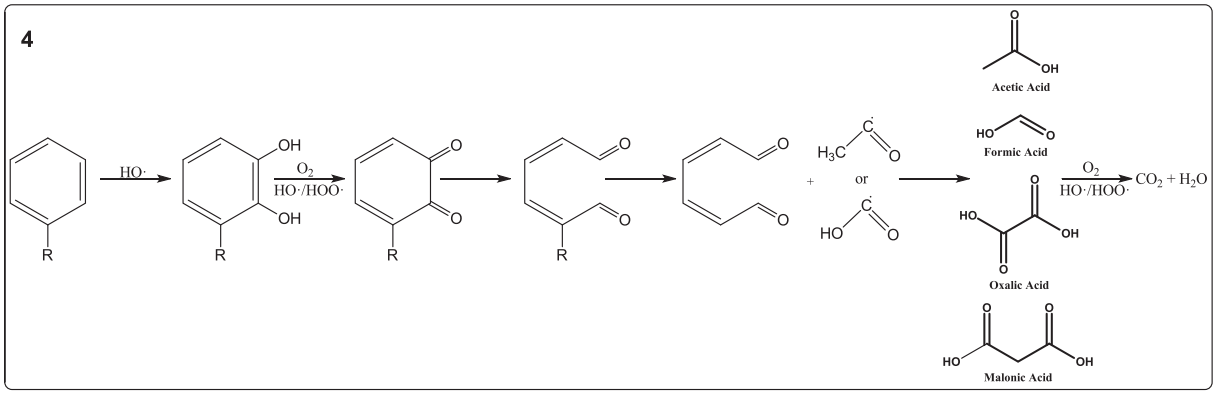

Fig. 9. Termination pathway of polystyrene degradation upon photo-Fenton treatment, including mineralization to CO_2 and H_2O. The molecules in bold represent the detected compounds in this work.

[54] which we have also identified using ion chromatography. In the final step, these short-chain acids are completely oxidized to CO_2 and H_2O [56–58]. Ultimately, it is important to highlight that at the end of the photo-Fenton reactions, complete mineralization of PS NPs and their leached oxidation by-products was achieved, as confirmed by TOC analyses, which measured levels below 0.1 mg L^{-1}, and TEM imaging, which revealed no remaining particles. This aspect is crucial, as the release of oxidized smaller NPs after the treatment could pose an even greater environmental hazard than pristine NPs [59]. In this context, future studies incorporating quantitative determination of the detected intermediates would further strengthen mechanistic understanding and provide deeper insights into the degradation pathways of NPs [60].

4. Conclusions

The photo-Fenton process has proven to be a highly efficient technology for the removal and complete mineralization of PS NPs from water. Surface-to-volume (S/V) ratio stands out as the determining factor of treatment effectiveness: higher S/V ratios correspond to faster nanoparticle degradation. This outcome is directly linked to the decomposition mechanism, which proceeds from the particle surface towards its core until complete elimination.

The experimental results were successfully described using the Shrinking Core Model and the Prout-Tompkins model. In addition, these mathematical models provide a powerful tool not only to interpret degradation kinetics but also to predict nanoplastic behavior under different conditions, thus contributing to the design and optimization of advanced treatment processes.

The degradation mechanism proposed in this study provides a comprehensive understanding of how PS nanoparticles oxidize under photo-Fenton conditions and consists of three distinct stages. During the initiation stage, the nanoparticles are activated and acquire reactive surface functionalities. In the propagation stage, a series of addition, extraction, and cleavage reactions transform the original polymer chains into lower molecular weight aromatic and aliphatic compounds. Finally, during the termination stage, these simpler compounds are completely mineralized into carbon dioxide and water, marking the end of the degradation process. This sequential pathway, supported by the identification of intermediate compounds using Py-GC/MS and IC analysis, confirms that all oxidation products evolve towards complete mineralization. These findings reinforce the environmental safety of the photo-Fenton process, as they ensure that no persistent, potentially toxic by-products or smaller particles remain after treatment.

CRediT authorship contribution statement

Jorge Garcia: Writing – review & editing, Writing – original draft, Visualization, Methodology, Investigation, Formal analysis, Conceptualization. **Carla di Luca:** Writing – review & editing, Visualization, Validation, Supervision, Methodology, Investigation. **Amina Abarkan:** Visualization, Methodology, Investigation. **Laura Cherta:** Validation, Methodology, Investigation. **Macarena Munoz:** Writing – review & editing, Writing – original draft, Project administration, Funding acquisition, Formal analysis, Conceptualization. **Zahara M. de Pedro:** Writing – review & editing, Supervision, Project administration, Funding acquisition, Conceptualization. **Jose A. Casas:** Writing – review & editing, Supervision, Project administration, Funding acquisition, Conceptualization.

Declaration of competing interest

The authors declare that they have no known competing financial interests or personal relationships that could have appeared to influence the work reported in this paper.

Acknowledgments

This research was supported by the Autónoma University of Madrid and the Community of Madrid through the project SI1-PJI-2019-00006, and by the Spanish Ministry for Science and Innovation through the project TED2021–131380B-C21 and PID2022-139063OB-I00, funded by MCIN/AEI/10.13039/501100011033 and, as appropriate, by "ERDF A way of making Europe" and by the European Union.

Appendix A. Supplementary data

Supplementary data to this article can be found online at https://doi.org/10.1016/j.jwpe.2025.108838.

Data availability

Data will be made available on request.

References

[1] G. Lamichhane, et al., Microplastics in environment: global concern, challenges, and controlling measures, Int. J. Environ. Sci. Technol. 20 (4) (2023) 4673–4694.
[2] J. Gigault, et al., Current opinion: what is a nanoplastic? Environ. Pollut. 235 (2018) 1030–1034.
[3] N.B. Hartmann, et al., Are we speaking the same language? Recommendations for a definition and categorization framework for plastic debris, Environ. Sci. Technol. 53 (3) (2019) 1039–1047.
[4] D. Liang, et al., Analysis, risk assessment and treatment of aquatic micro/nanoplastics: a critical review, Sep. Purif. Technol. 354 (2025) 129418.
[5] M. Sadia, et al., Microplastics pollution from wastewater treatment plants: a critical review on challenges, detection, sustainable removal techniques and circular economy, Environ. Technol. Innov. 28 (2022) 102946.

[6] S. Monira, et al., Nano and microplastics occurrence in wastewater treatment plants: a comprehensive understanding of microplastics fragmentation and their removal, Chemosphere 334 (2023) 139011.
[7] Z. Song, et al., Fate and transport of nanoplastics in complex natural aquifer media: effect of particle size and surface functionalization, Sci. Total Environ. 669 (2019) 120–128.
[8] S. Lambert, M. Wagner, Characterisation of nanoplastics during the degradation of polystyrene, Chemosphere 145 (2016) 265–268.
[9] J. Sun, et al., Microplastics in wastewater treatment plants: detection, occurrence and removal, Water Res. 152 (2019) 21–37.
[10] G. Bhavya, et al., Remediation of emerging environmental pollutants: a review based on advances in the uses of eco-friendly biofabricated nanomaterials, Chemosphere 275 (2021) 129975.
[11] M. Keerthana Devi, et al., Removal of nanoplastics in water treatment processes: a review, Sci. Total Environ. 845 (2022) 157168.
[12] J. Li, H. Liu, J. Paul Chen, Microplastics in freshwater systems: a review on occurrence, environmental effects, and methods for microplastics detection, Water Res. 137 (2018) 362–374.
[13] S. Kim, et al., Advanced oxidation processes for microplastics degradation: a recent trend, Chem. Eng. J. Adv. 9 (2022) 100213.
[14] Gomes de Aragão, T. Belé, et al., Oxidation of microplastics by O3 and O3/H2O2: surface modification and adsorption capacity, J. Water Process Eng. 41 (2021) 102072.
[15] M. Munoz, et al., Adsorption of micropollutants onto realistic microplastics: role of microplastic nature, size, age, and NOM fouling, Chemosphere 283 (2021) 131085.
[16] K. Zhu, et al., Long-term phototransformation of microplastics under simulated sunlight irradiation in aquatic environments: roles of reactive oxygen species, Water Res. 173 (2020) 115564.
[17] J. Lin, et al., Effect of degradable microplastics, biochar and their coexistence on soil organic matter decomposition: a critical review, TrAC Trends Anal. Chem. 183 (2025) 118082.
[18] Y. Li, et al., Degradation of nano-sized polystyrene plastics by ozonation or chlorination in drinking water disinfection processes, Chem. Eng. J. 427 (2022) 131690.
[19] H. Hidayaturrahman, T.-G. Lee, A study on characteristics of microplastic in wastewater of South Korea: identification, quantification, and fate of microplastics during treatment process, Mar. Pollut. Bull. 146 (2019) 696–702.
[20] A.D. Vital-Grappin, et al., The role of the reactive species involved in the photocatalytic degradation of HDPE microplastics using C,N-TiO2 powders, Polymers 13 (7) (2021) 999.
[21] D.A. Maulana, M. Ibadurrohman, Slamet, Synthesis of nano-composite ag/TiO2 for polyethylene microplastic degradation applications, IOP Conf. Ser.: Mater. Sci. Eng. 1011 (1) (2021) 012054.
[22] M. Kiendrebeogo, et al., Nanoplastics removal from spiked laundry wastewater using electro-peroxidation process, Chemosphere 341 (2023) 139963.
[23] D. Ortiz, et al., Insights into the degradation of microplastics by Fenton oxidation: from surface modification to mineralization, Chemosphere 309 (2022) 136809.
[24] C. di Luca, et al., Mineralization of polystyrene nanoplastics in water by photo-Fenton oxidation, J. Environ. Chem. Eng. 11 (5) (2023).
[25] C. di Luca, et al., Strategies for the quantification and characterization of nanoplastics in AOPs research, Chem. Eng. J. 493 (2024) 152490.
[26] J.J. Pignatello, E. Oliveros, A. MacKay, Advanced oxidation processes for organic contaminant destruction based on the Fenton reaction and related chemistry, Crit. Rev. Environ. Sci. Technol. 36 (1) (2006) 1–84.
[27] J. Carbajo, et al., Increasing photo-Fenton process efficiency: the effect of high temperatures, Sep. Purif. Technol. 271 (2021) 118876.
[28] M. Li, et al., VUV/UV light inducing accelerated phenol degradation with a low electric input, RSC Adv. 7 (13) (2017) 7640–7647.
[29] K. Zoschke, H. Börnick, E. Worch, Vacuum-UV radiation at 185 nm in water treatment – a review, Water Res. 52 (2014) 131–145.
[30] R. Ameta, et al., Fenton and photo-Fenton processes, in: Advanced Oxidation Processes for Waste Water Treatment, Elsevier, 2018, pp. 49–87.
[31] S. Malato, et al., Decontamination and disinfection of water by solar photocatalysis: recent overview and trends, Catal. Today 147 (1) (2009) 1–59.
[32] D. Spasiano, et al., Solar photocatalysis: materials, reactors, some commercial, and pre-industrialized applications. A comprehensive approach, Appl. Catal. B Environ. 170-171 (2015) 90–123.
[33] C. di Luca, et al., Modeling polystyrene nanoplastics degradation in water via photo-Fenton treatment: a shrinking-particle approach, Appl. Catal. B: Environ. Energy 362 (2025) 124751.
[34] G. Eisenberg, Colorimetric determination of hydrogen peroxide, Ind. Eng. Chem. Anal. Ed. 15 (5) (1943) 327–328.
[35] E.B. Sandell, Colorimetric determination of traces of metals, Soil Sci. 101 (2620) (1945) 275–276.
[36] L.P. Domínguez-Jaimes, et al., Degradation of primary nanoplastics by photocatalysis using different anodized TiO2 structures, J. Hazard. Mater. 413 (2021) 125452.
[37] E. Yousif, R. Haddad, Photodegradation and photostabilization of polymers, especially polystyrene: review, SpringerPlus. 2 (2013) 398.
[38] A. Pérez-López, et al., Removal of polystyrene nanoplastics from urban treated wastewater by electrochemical oxidation, Sep. Purif. Technol. 363 (2025) 132139.
[39] Y. Cai, et al., Degradation of polystyrene nanoplastics in UV/NaClO and UV/PMS systems: insights into degradation efficiency, mechanism, and toxicity evaluation, Water 15 (10) (2023) 1920.
[40] Q. Ye, et al., Advanced polystyrene nanoplastic remediation through electro-Fenton process: degradation mechanisms and pathways, J. Environ. Chem. Eng. 13 (5) (2025) 118907.
[41] K. Yin, et al., A comparative review of microplastics and nanoplastics: toxicity hazards on digestive, reproductive and nervous system, Sci. Total Environ. 774 (2021) 145758.
[42] M.E. Brown, The Prout-Tompkins rate equation in solid-state kinetics, Thermochim. Acta 300 (1–2) (1997) 93–106.
[43] E.G. Prout, F.C. Tompkins, The thermal decomposition of potassium permanganate, Trans. Faraday Soc. 40 (1944) 488.
[44] A.L. Angulo, C.L.C. Rodriguez, G.J.M. Fechine, Photooxidative behavior of polystyrene nanocomposites filled with two-dimensional molybdenum disulfide, Polymers 15 (9) (2023) 2099.
[45] J.-L. Gardette, B. Mailhot, J. Lemaire, Photooxidation mechanisms of styrenic polymers, Polym. Degrad. Stab. 48 (3) (1995) 457–470.
[46] X. Shi, et al., The photochemical behaviors of microplastics through the lens of reactive oxygen species: photolysis mechanisms and enhancing photo-transformation of pollutants, Sci. Total Environ. 846 (2022) 157498.
[47] S. Dinoop lal, T. Sunil Jose, C. Rajesh, Solid-phase photodegradation of polystyrene by nano TiO2 under ultraviolet radiation, Environ. Nanotechnol. Monitor. Manag. 12 (2019) 100229.
[48] Z. Peng, R. Chen, H. Li, Heterogeneous photocatalytic oxidative cleavage of polystyrene to aromatics at room temperature, ACS Sustain. Chem. Eng. 11 (29) (2023) 10688–10697.
[49] A. Severino, et al., Integrated nanofiltration and photocatalytic processes for the removal of polystyrene nanoplastics waste in water, Sep. Purif. Technol. 360 (2025) 131232.
[50] J. Shang, M. Chai, Y. Zhu, Photocatalytic degradation of polystyrene plastic under fluorescent light, Environ. Sci. Technol. 37 (19) (2003) 4494–4499.
[51] X. Wu, et al., New insights into the photo-degraded polystyrene microplastic: effect on the release of volatile organic compounds, J. Hazard. Mater. 431 (2022) 128523.
[52] E. Brillas, S. Garcia-Segura, Benchmarking recent advances and innovative technology approaches of Fenton, photo-Fenton, electro-Fenton, and related processes: a review on the relevance of phenol as model molecule, Sep. Purif. Technol. 237 (2020) 116337.
[53] P. García-Muñoz, et al., Photocatalytic degradation of polystyrene nanoplastics in water. A methodological study, J. Environ. Chem. Eng. 10 (4) (2022).
[54] R. Singla, M. Ashokkumar, F. Grieser, The mechanism of the sonochemical degradation of benzoic acid in aqueous solutions, Res. Chem. Intermed. 30 (7–8) (2004) 723–733.
[55] B. Yang, A. Liang, L. Wang, The atmospheric oxidation mechanism of acetophenone initiated by the hydroxyl radicals, Atmos. Environ. 309 (2023) 119905.
[56] Y. Ogata, K. Tomizawa, Y. Yamashita, Photoinduced oxidation of benzoic acid with aqueous hydrogen peroxide, J. Chem. Soc. Perkin Trans. 2 (4) (1980) 616.
[57] M.A. Oturan, et al., Reaction sequence for the mineralization of the short-chain carboxylic acids usually formed upon cleavage of aromatics during electrochemical Fenton treatment, Electrochim. Acta 54 (2) (2008) 173–182.
[58] Q. Sun, et al., Comparison of the reactivity of nanosized zero-valent iron (NZVI) particles produced by borohydride and dithionite reduction of iron salts, Nano 03 (05) (2008) 341–349.
[59] E.D. Tsochatzis, et al., Microplastics and nanoplastics: exposure and toxicological effects require important analysis considerations, Heliyon 10 (11) (2024).
[60] Y. Tang, et al., Synergetic effect of in-situ CaO on PVC plastic pyrolysis characteristics: TG and Py GC/MS analysis, Polym. Degrad. Stab. 234 (2025) 111205.